AERODYNAMIC SHAPE OPTIMIZATION OF TILTROTOR BLADES EQUIPPED WITH CONTINUOUS MORPHING AEROFOILS

Antonio Pagano, CIRA, Italian Aerospace Research Centre, Capua (CE), Italy

Abstract

This document explores the adoption of morphing blades on tiltrotors with the aim of improving the rotor aerodynamic performance. Rotors for such aircrafts are designed to simultaneously address the peculiarities of both axial flights (hover, vertical ascent/descent and cruise) and edge flights (flyover). Some of the current aerofoil morphing technologies are investigated from the aerodynamic point of view so that the blade can modify its shape to meet the best rotor performance for the examined flight conditions. The potential benefits are discussed through the application of numerical procedures on a realistic tiltrotor geometry.

1. INTRODUCTION

The paper explores the potential of continuous morphing aerofoils when incorporated within a tiltrotor blade.

Continuous morphing aerofoils are able to modify their aerodynamic characteristics by a continuous change in their shape without gaps or surface discontinuities. Among all of the concepts appeared in the recent literature,[1-6] herein are considered those continuous morphing aerofoils obtained by installing devices whose activation, separately or simultaneously, induces leading edge deformation, trailing edge deformation and static trailing edge extension. Thanks to the lack of gaps between fixed and moveable parts of aerofoils, the morphing devices have an improved efficiency, as discussed in [7] where deformable trailing edges and discrete trailing edge flaps are compared.

Tiltrotor blades which experience a significant number of flow conditions depending on the aircraft operative mode (helicopter, airplane and conversion mode) have a shape usually obtained by means of an aerodynamic passive optimization on conflicting requirements. This optimization tends to select blade designs characterized by longer rotor radii and larger blade areas, as consequence of a high loads demand in helicopter mode. This has an impact on high speed level flight where rotors should be smaller to gain more efficiency since it is in that flight regime that the tiltrotor is expected to spend much of its mission profile.

In addition, a large rotor diameter significantly influences the aircraft configuration and safety issues are of some concern. The tiltrotor European concept ERICA[8] has been conceived on a reduced rotor diameter so that the tiltrotor can also take-off and land as a propeller driven aircraft. DART[9], ADYN[10] and NICETRIP[11]-[12] are past European Commission funded projects concentrating on the ERICA concept.

In the context of morphing technology, retractable and telescopic rotors are lately become less attractive especially with the appearance of variable speed rotors. On the other hand, concepts on continuous variable geometry aerofoils are emerging and many of them are successfully progressed to the prototype status. Many of these concepts allow, with respect to the un-morphed geometry, for a lift increase which may be used to respond to the high thrust demand of tiltrotor blade sections in hover. Thus, their incorporation within a tiltrotor blade, especially if the correspondent blade morphing is considered since the early stage of design, may lead to significant aerodynamic performance improvements since the compromise between hover and cruise requirements is no longer so stringent.

2. BACKGROUND AND ACTUAL FOCUS

CIRA past activities on aerodynamic shape optimization of tiltrotor blades were articulated on two steps: the assessment of an efficient simulation environment[13] and the review of numerical investigations where planform, twist, angular velocity, rotor radius and aerofoil placements were simultaneously involved.[14] The assembly of code networks for rotor performance calculations and the optimization strategy[13] deserved a great attention to make the whole optimization task affordable. In particular, a flexible integration environment was built based on the possibility of selecting the most convenient analysis tools by balancing them with the resulting increased simulation complexity and computational effort. After its assessment, that environment was applied to an optimization study[14] where new blade designs for variable diameter and variable speed tiltrotors were obtained giving

evidence of the benefits arising from the performed blade shape optimization. One of the findings was that a different spanwise aerofoil distribution allowed for improved performance at design points both in hover and in cruise operative conditions, but the hover performance suddenly degraded as the blade load increased.

The subsequent steps are the object of the paper here proposed. High loaded conditions in hover can be achieved by the activation of devices which change the blade shape. To meet the goal of optimizing the blade in presence of morphing cross sections, techniques for continuously deforming aerofoil geometries have been used to obtain leading edge deformations (LED), trailing edge deformations (TED) and static extended trailing edge (SETE[1]) geometries; the resulting aerofoils have been aerodynamically characterized both for an isolated device or a combination of them; the strategy that allows different aerofoils to be included in an optimization task has been implemented into an automatic numerical process by exploiting the two level optimization feature of the Optimus® multi-disciplinary design optimization software.[17] The above described developments have been applied on the tiltrotor blade designed within the ADYN project.[10]

The nature of the performed investigations was exploratory and the complexity of the device mechanisms and the power absorbed by them was not considered. The focus was on the aerodynamic efficiency and on the aerofoil selection. In fact, it was expected to select and to place along the blade span those aerofoils whose shape led to the best performance both in cruise when the blade is un-morphed and in hover when a morphing device is activated. The kind of morphing device was not know in advance as well as the amount of deformation to be applied.

To meet the goals illustrated above, past developments were largely exploited. References [13]-[14] contain the description of the numerical processes and the mathematical models which the reader is asked to refer to for details. Nevertheless, some modifications were necessary and they are illustrated in sections 3-6 of this paper. Section 7 is dedicated to the discussion of the results obtained from the investigation of a case study.

3. AIRFOIL SELECTION

In [14] the strategy to select aerofoils for un-morphed blades has been described in details. Fundamentally, the blade geometry was constructed by the information contained into two separate input files: the first one with the planform data (including twist) and the other with the aerofoil shape. Thus, a blade with a given planform could be equipped with different aerofoils shapes and spanwise distributions. The module dealing with aerofoil selection and distribution has been modified to accommodate the treatment of either morphing and non-morphing sections. Basically, a ASCII file (blade model) was used to set the available aerofoils (that is, the name of the files with their non-dimensional geometry and the associated aerodynamic look-up table), an initial guess of the spanwise position and the number of morphing states if any.

n	Segment1	Segment2	Segment3
1	A-A	-	-
2	B-B	-	-
3	A-B	-	-
4	A-A	A-B	-
5	A-B	B-B	-
6	A-A	A-B	B-B

Table 1: different blade models from aerofoils A and B.

A morphing state, that is, a modified aerofoil shape resulting from the morphing device activation, was characterized, as any other aerofoil, by the geometry and the aerodynamic look up table. The module produced the list of all the blade models with different combinations of aerofoils and segments as output. The strategy was based on some driving factors hereafter described:

- one aerofoil results into one blade segment corresponding to the blade span;
- two or more different aerofoils generate several blade segments;
- at this stage, a blade segment is only characterized by its length and the aerofoil shapes;
- if two consecutive aerofoils have different geometries, three blade segments are introduced so that two segments have a constant aerofoil and the third in the middle allows for the transition to an aerofoil geometry to the subsequent one;
- the number of blade models depends on the number of aerofoils (two geometrically different aerofoils, A and B, may originate six blade models as illustrated in Table 1);
- if an aerofoil has several morphing states, as many blade models are generated as the number of morphing states;
- the user has the possibility of excluding those segments which have two different morphing states at their external sections;

[1] The acronym is used in [15]-[16].

- the more different aerofoils (and morphing states) are used the more the number of possible blade models;
- the aerofoil chord-to-ratio thickness cannot increase as its spanwise position progresses towards the blade tip;
- the length of blade segments are modified by the module dealing with blade parameterization.

4. MORPHING TECHNIQUES

Among the techniques to morph an aerofoil geometry, a smooth deformation has been applied to induce a nose droop or a continuous trailing edge flap. In particular, the aerofoil part to be deformed is split in two so that one is rigidly rotated and the other accommodates the deformation of the nose or the trailing edge. With reference to Figure 1, the rotation Ψ_{LED} affects the points of the segment comprised between x_{rig} and x_{rot} according to the following law:

$$\Psi_i = \Psi_{LED}\left(\frac{x_{rot}-x}{x_{rot}-x_{rig}}\right)^{\frac{2}{3}}.$$

This strategy allows to preserve the shape of both leading and trailing edge. The points x_{rig} and x_{rot} can be set by the user. For the present application they correspond, respectively, to 10% and 25% of the chord.

Concerning the device based on SETE, a flat plate of length x_{SETE} and thickness equal to the trailing edge thickness can extend out of the trailing edge according to an user defined angle mainly depending on the available internal volume. Both the chordwise plate elongation ($\Delta_{SETE}=L_{SETE}/x_{SETE}$) and the associated angle (Ψ_{SETE}) can be set as illustrated in Figure 2.

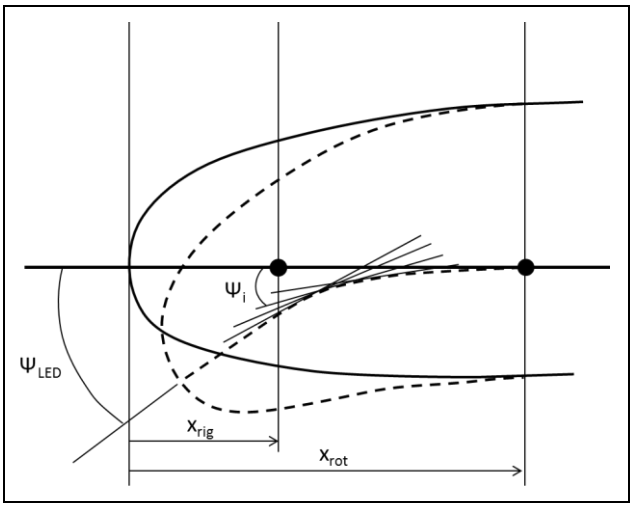

Figure 1: leading edge deformation.

A value of 20% of the chord is used for x_{SETE}. When the trailing edge includes a tab, the plate comes out as a natural elongation of the tab. The user has in this case the possibility of modify the tab angle. The aerofoil deformation is performed as an off-line activity and presently requires a visual inspection before proceeding with the aerodynamic characterization in order to be sure that any anomalous surface irregularity or any volume violation is not present.

5. BLADE SURFACE GENERATION

As anticipated before, sectional values for some noticeable quantities such as chord or built-in twist are specified by means of another ASCII file (blade constructive parameters). The blade surface generator firstly reads the blade model (with aerofoil shapes and radial distribution) and the constructive parameters and then each aerofoil geometry, depending on the actual radial position, is scaled according to the given chord, rotated of the specified built-in twist and so on for all of the constructive parameters. Thus, it is possible to obtain different blade surfaces by using the same constructive parameters (that is, the planform) and mounting different aerofoils (which may differ in shape and radial position).

6. AERODYNAMIC MODEL

The in-house CIRA BEMT code provides both the rotor trim and the performance evaluation. The BEMT code uses simplified aerodynamics which, for steady conditions, basically makes use of the 2D aerodynamic coefficients look-up tables and, for unsteady conditions, a Beddoes-Lieshman type state-space formulation.[18] Several approximations are used for the stall treatment and the flow three-dimensionality. Recently the BEMT code has been updated to remove some limitations,[19] mainly related to the small angles approximation, and to further improve the model with the inclusion of the swirl velocity.

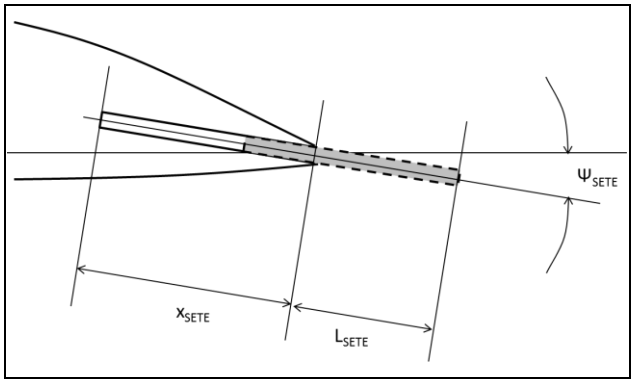

Figure 2: aerofoil deformation for SETE.

This section includes a brief description of the new mathematical model and its validation.

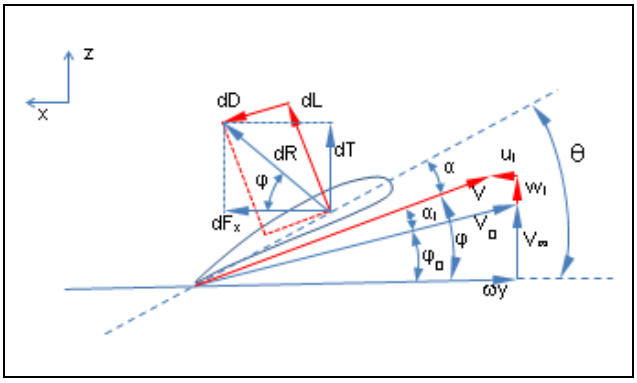

Figure 3: aerofoil under peripheral and free stream velocity.

6.1. Description

A blade aerofoil at a radial station *y* of a propeller of radius R which is advancing at a velocity V_∞ and rotating at a peripheral velocity ωy is exposed to a relative velocity

$$V = \sqrt{(V_\infty + w_i)^2 + (\omega y - u_i)^2}\ ,$$

where w_i and u_i are, respectively, the axial and tangential induced velocities. The inflow angle between the plane of rotation and V is

$$\varphi = \varphi_0 + \alpha_i = tg\,\frac{V_\infty}{\omega y} + \alpha_i\ .$$

By looking at Figure 3, the forces along the reference system axes can be computed as

$$\begin{cases} dT = dL\cos\varphi - dD\sin\varphi \\ dF_x = dL\sin\varphi + dD\cos\varphi \end{cases},$$

where the elementary lift and drag come from the blade element theory applied to a blade segment whose spanwise and chordwise dimensions are *dy* and c_y

$$\begin{cases} dL = {}^1\!/_2\,\rho V^2 c_y dy\, C_l \\ dD = {}^1\!/_2\,\rho V^2 c_y dy\, C_d \end{cases}.$$

The thrust and torque extracted from a rotor annulus, according to the momentum theory, are:

$$\begin{cases} dT = 4(1-B)\pi\rho y dy\,|V_\infty + w_i|\,w_i \\ dF_x = 4(1-B)\pi\rho y dy\,|V_\infty + w_i|\,u_i \end{cases},$$

where B is the Prandtl's tip los factor (N_b is the blade number):

$$B = \frac{2}{\pi}\cos^{-1}\left[exp\left(\frac{N_b\left(\frac{y}{R}-1\right)}{2\frac{y}{R}\sin\varphi}\right)\right].$$

By equating the elementary forces coming from the blade element and momentum theories, it is possible to obtain the following transcendental equations:

$$\begin{cases} \frac{V_\infty}{V} = \sin\varphi - \frac{1}{8B}\frac{N_b c_y}{\pi y}\frac{1}{\sin|\varphi|}\left[C_l\cos\varphi - C_d\sin\varphi\right] \\ \frac{\omega y}{V} = \cos\varphi + \frac{1}{8B}\frac{N_b c_y}{\pi y}\frac{1}{\sin|\varphi|}\left[C_l\sin\varphi + C_d\cos\varphi\right] \end{cases}.$$

When the right terms are called, respectively, F(φ) and G(φ), the transcendental equations can be rewritten as

$$\begin{cases} \frac{V_\infty}{V} = \mathrm{F}(\varphi) \\ \frac{\omega y}{V} = \mathrm{G}(\varphi) \end{cases}.$$

These two equations are subsequently combined into a single transcendental equation by extracting V from each of them and then subtracting:

$$V - V = 0 = F(\varphi) - \frac{V_\infty}{\omega y}G(\varphi)\ .$$

Its complete form is:

$$\left(\sin\varphi - \frac{V_\infty}{\omega y}\cos\varphi\right)\sin\varphi - \sin|\varphi|\ \frac{1}{8B}\frac{N_b c_y}{\pi y}$$
$$\left[C_l\left(\cos\varphi + \frac{V_\infty}{\omega y}\sin\varphi\right) - C_d\left(\sin\varphi - \frac{V_\infty}{\omega y}\cos\varphi\right)\right] = 0.$$

This equation is solved by means of the *regula falsi* method.[20] Once φ is known, V is calculated and the axial induced velocity and the swirl velocity are computed as:

$$\begin{cases} w_i = V\sin\varphi - V_\infty \\ u_i = \omega y - V\cos\varphi \end{cases}.$$

6.2. Validation

With reference to tiltrotor configurations, Figure 4 includes the comparisons on the rotor performance of numerical predictions against the experimental data of the ADYN test campaign.

The rotational tip velocity is $M_{\Omega R}$=0.504 in hover and $M_{\Omega R}$=0.491 in cruise; the Wind Tunnel flow velocity is M_{WT}=0 in hover and M_{WT}=0.30 in cruise. The results shown in this figure comes from the postdictive phase when the code was trained with the help of experimental and CFD data.

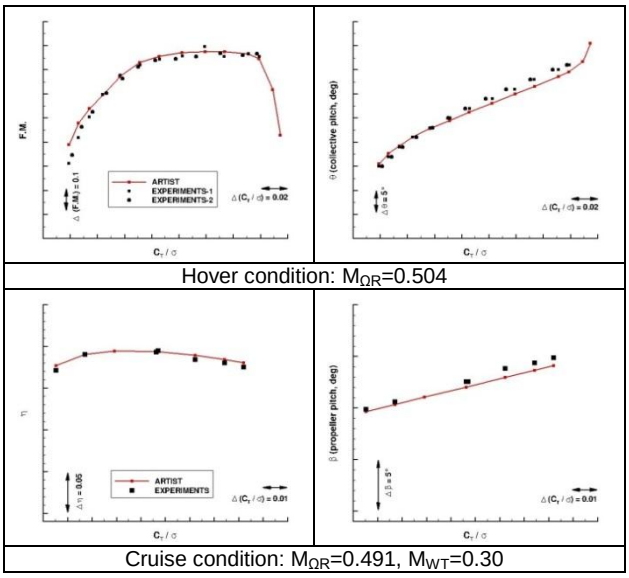

Figure 4: validation of the BEMT code on the ADYN rotor.

Recently, in the framework of the European Commission funded project ESPOSA,[21] an experimental analysis of the effect of non-uniform inflow conditions on the performance of propellers was performed by conducting two test campaigns: the first one at DNW-LST wind tunnel on a 4-bladed propeller and the second one at the TUD-OJF facility on a 8-bladed propeller.

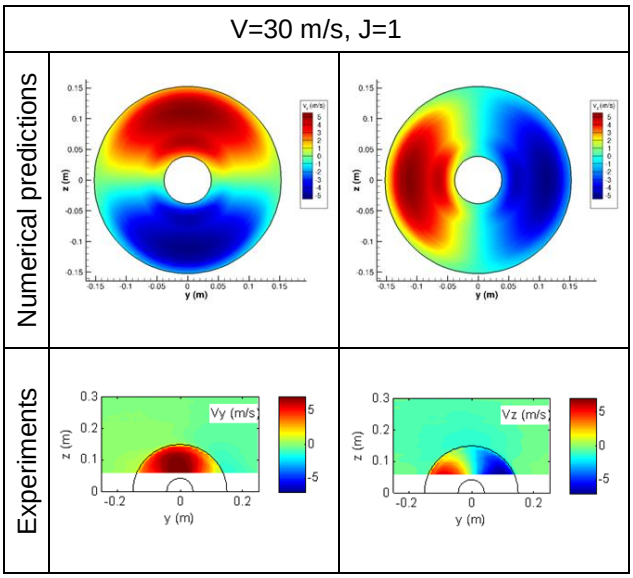

Figure 5: comparison of the velocity components; numerical results are obtained in the propeller disk, experiments refer to data at a distance of 56 mm from the disk.

Both propellers were assembled by adopting the same blade but they were installed into different wind tunnel models. The propellers were basically tested at a fixed pitch, under two free stream velocities (30 and 60 m/s), for several angular velocities spanning from 3000 rpm to 11000 rpm and with flow unsteadiness coming either from a non-zero angle between the propeller axis and the free stream either from the presence of a wing downstream the propeller. The velocity components behind the propellers were also measured and the comparison with CIRA BEMT code is illustrated in Figure 5. The calculations on the two model propellers reveal a fairly good agreement with experiments in terms of thrust and torque (see also Figure 6 and Figure 7). At lower advance ratios the CIRA BEMT code predicts, especially for the 4-bladed propeller, high sectional effective angles of attack which imply the aerofoils work well beyond the stall angle.

7. CASE STUDY

The paper refers to the broad context of 3D aerodynamic shape optimization of rotary wing propulsion systems. Nevertheless, the un-morphed sectional aerofoil geometry is considered as a not modifiable entity because of the wide range of angles of attack and Mach number it is exposed to and because of the fundamental intrinsic unsteady nature of the flow. In fact, aerofoil optimization is often treated as a separate problem which deserves specialist analyses.

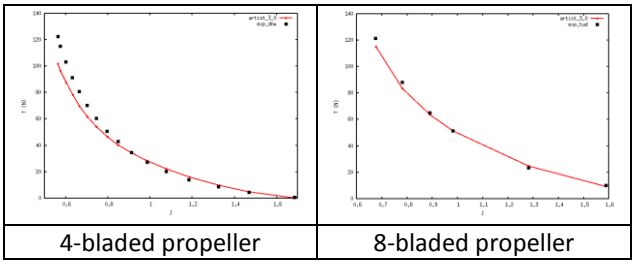

Figure 6: Propeller thrust vs advance ratio.

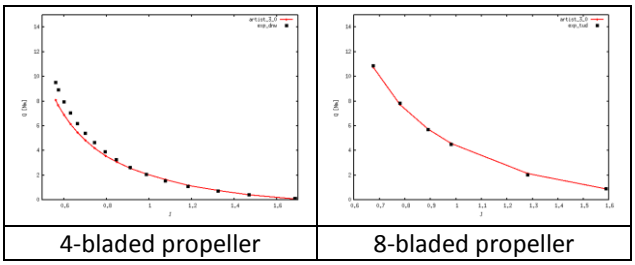

Figure 7: Propeller torque vs advance ratio.

In addition, maintaining the aerofoil geometry unchanged is a necessary condition for this study since the shape of the aerofoil has a direct link to the available internal space on which depends the accommodation of the morphing device. Despite this assumption, the optimization here performed can still be considered three-dimensional since the un-morphed aerofoil geometry can be selected among a

given set of aerofoils, its spanwise position can be appropriately determined and its shape can be varied as a consequence of the deformations introduced by pre-selected continuous morphing shape devices. The blade shape is optimized to maximize the aerodynamic rotor performance in helicopter and airplane operational modes. The morphing devices are assumed to be activated only for hovering.

7.1. Baseline geometry

In the framework of the European Commission funded research projects TILTAERO[22] and ADYN[10], an articulated experimental campaign was conducted on the ERICA rotor and on its aero-acoustically optimized version, the ADYN rotor. This rotor, described in [23], was subsequently selected to equip a tiltrotor model (full configuration) under investigation in the project NICETRIP. [24] The ADYN model rotor has a diameter of about 3 m and the blades are characterized by a double sweep angle, with anhedral angle at the tip and a complex non-linear twist and chord span distribution.[25] Its blade, limited to the aerodynamic part (from r/R=0.25 to the tip, as illustrated in Figure 8) has been used for this exercise.

Aerofoil	t/c	$C_{l\,max}$	C_d @ C_l=0	M_{dd} @ C_l=0
A1	0.35	1.14 *(M=0.3)*	0.016 *(M=0.3)*	0.60
A2	0.20	1.84 *(M=0.3)*	0.00825 *(M=0.4)*	0.70
A3	0.12	1.52 *(M=0.3)*	0.00795 *(M=0.6)*	0.79
A4	0.09	1.35 *(M=0.3)*	0.00741 *(M=0.6)*	0.83
A5	0.07	1.24 *(M=0.3)*	0.00727 *(M=0.6)*	0.86

Table 2: aerofoil performance.

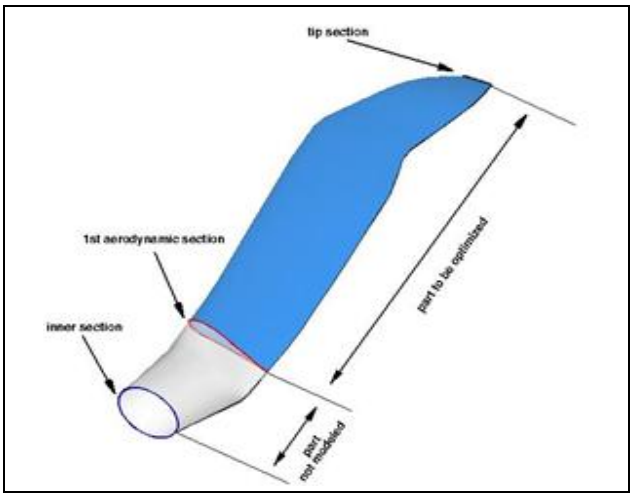

Figure 8: 3D view of the ADYN blade.

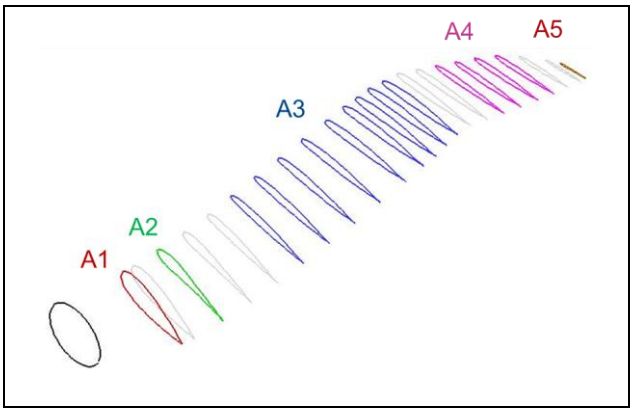

Figure 9: aerofoil and segment distribution of the baseline blade. Different colours stand for different aerofoil shapes. Grey colour is for transitional aerofoils.

The blade model is based on the distribution of the aerofoils listed in Table 2 over seven segments as depicted in Figure 9.

7.2. Optimization objectives

The rotor blade is optimized so that the aerodynamic performance is maximized at two nominal rotor load conditions: in hover flight, and the thrust coefficient is C_T=0.021 at a rotational tip velocity (in terms of Mach number) of $M_{\Omega R}$=0.63; in level flight the thrust coefficient is C_T=0.0157 at a rotational tip velocity of $M_{\Omega R}$=0.532 and at an advance flight velocity of M_{WT}=0.58 (350 Kn at 7500 m).

7.3. Morphing states

The use of devices for modifying the blade sectional geometry on rotorcraft configurations is largely debated. For example, in [26] the pro and cons of trailing edge extension, trailing edge flap and Gurney flap are reviewed; leading edge and trailing edge deflections are studied in [27]-[28] for helicopter performance enhancement.

Among the aerofoils specified in Table 2, the aerofoil with 12% thickness-to-chord ratio has been selected for the application of the morphing techniques described in section 4. The applied deformations, which are summarised in Table 3, originate from literature review. In particular, the aerofoil nose was drooped by 10°, 15° and 20°; three different rotations were set for the trailing edge (2.5°, 5° and 10°); the trailing edge plate extended by 60%, 75% or 90% of its length which was based on 20% of the local chord. The aerofoil geometries resulting from the separate application of the morphing devices are depicted in Figure 10.

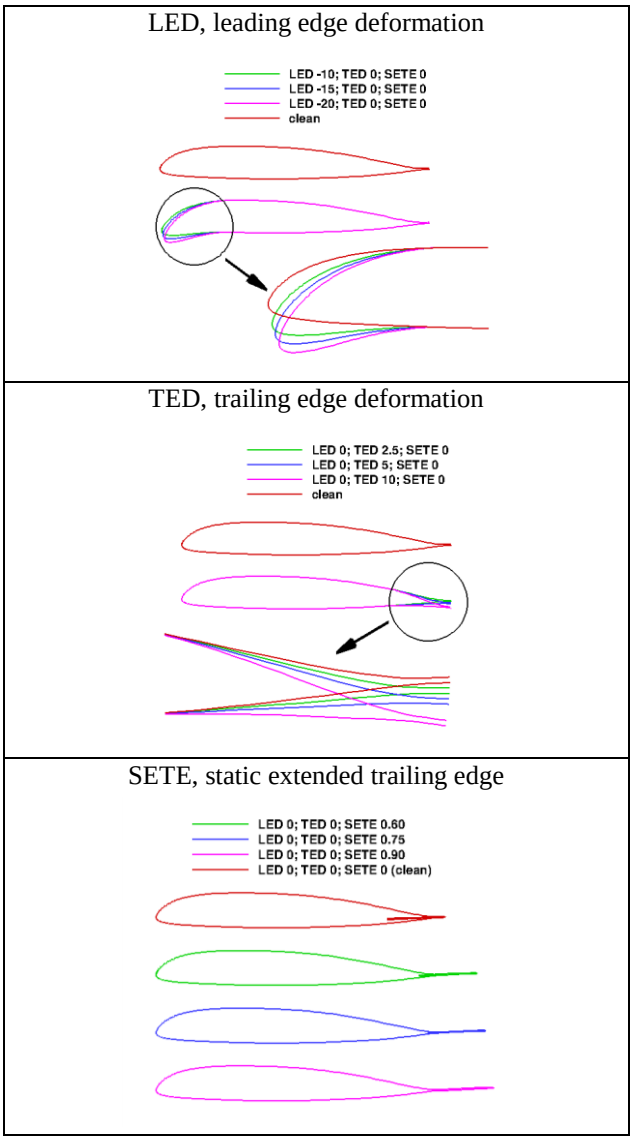

Figure 10: continuous morphing aerofoil shapes.

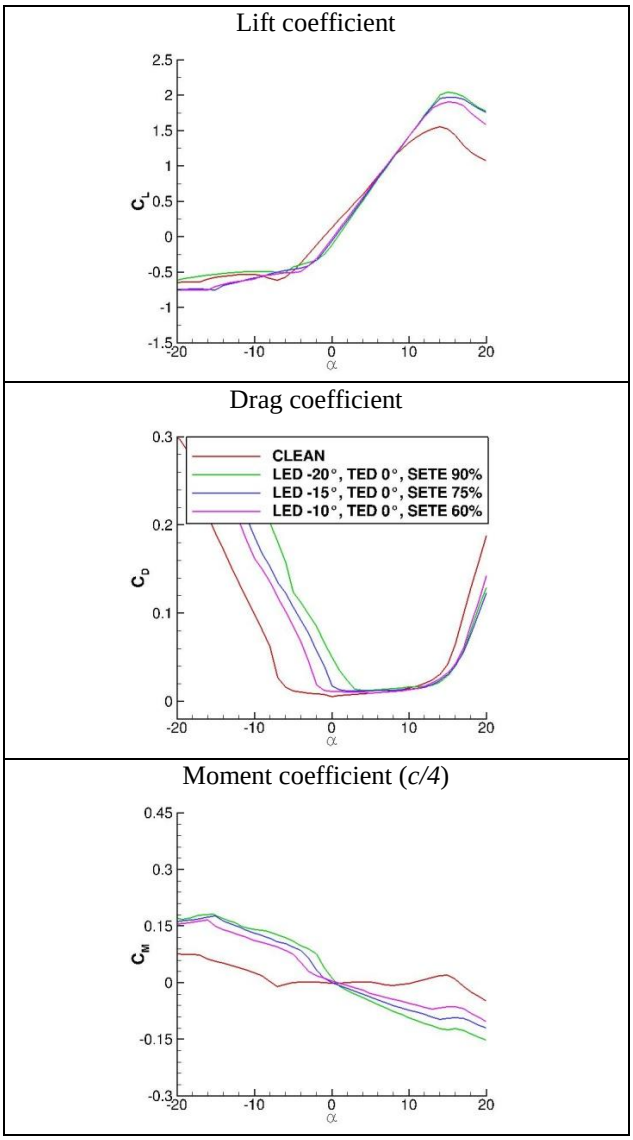

Figure 11: aerodynamic characterization of a section with multiple morphing devices at Mach=0.4

Id.	Ψ_{LED}	Ψ_{TED}	Δ_{SETE}
A3_00	0	0.0	0.0
A3_01	10	-	-
A3_02	15	-	-
A3_03	20	-	-
A3_04	-	2.5	-
A3_05	-	5.0	-
A3_06	-	10.0	-
A3_07	-	-	0.60
A3_08	-	-	0.75
A3_09	-	-	0.90
A3_10	10	-	0.60
A3_11	15	-	0.75
A3_12	20	-	0.90
A3_13	10	-2.0	0.60

Table 3: morphing deformations applied on aerofoil A3

Table 3 also includes multiple deformations coming from the combination of different devices.

All of the morphing states listed in Table 3 (thus, including the clean aerofoil) have been numerically characterized and the relative look-up tables have been computed by using a Euler/Boundary layer code. Figure 11 compares the aerofoil performance for the A3_10-A3_12 morphed shapes of Table 3.

7.4. Code integration and optimization environment

In the present study Optimus® has been used both as code integration tool and as optimization environment. Figure 12 captures the numerical process used to compute the hover performance

over a given range of loads. Analogous processes have been built for pitch or RPM sweeping. To evaluate the hover and cruise performance of a given list of blade models, the process in Figure 13 has been used. The optimization task has been accomplished by exploiting the Optimus in Optimus® tool which allows to perform an optimization on top of another optimization. In fact, some design variables affected the blade shape in both operative modes (hover and cruise). On the contrary, the aerofoil geometry (which of course is always the same) is morphed in hover but is not in cruise.

Figure 14 illustrates the numerical process when Optimus in Optimus® is invoked. The icon representing Optimus in Optimus® comprises the processes illustrated in Figure 15 and Figure 16, which are referred as tasklists according to the Optimus® nomenclature.

7.5. Results

The performance of the baseline rotor has been recomputed because of the look-up tables which were homogenously obtained by the same CFD code and at the appropriate Reynolds numbers. Figure 17 gives evidence that the hover performance rapidly degrades after the thrust nominal value. The first investigation which was performed aimed at seeing whether the activation of morphing devices was able to ensure safer margins. The aerofoil selection module has been run starting from the aerofoils equipping the baseline blade (five, in total) one of them with 13 morphing states. The module gave as output a list of 1649 possible blade models where the blade segments were not yet optimized. The process of Figure 13 has been launched with the goal of exploring all of the available designs at nominal conditions except for the hover thrust which was increased by the 20% with respect to the nominal value. The analysis of Figure 18 allows to see that the designs fulfilling the thrust increase in hover were both equipped with un-morphed and morphed sections. If some of them succeeded by just positioning differently the aerofoils (as already observed in [14]), the number of those implementing morphing aerofoils was significantly higher.

After sorting the best design with improved propeller efficiency and figure of merit, its performance has been compared with that of the baseline rotor in Figure 19. That design which was identified by the label 285 basically presented the following differences with respect to the baseline blade: the absence of aerofoil A2, the replacement of aerofoil A3 with A3_01 and the blade tip equipped by the A_4 aerofoil.

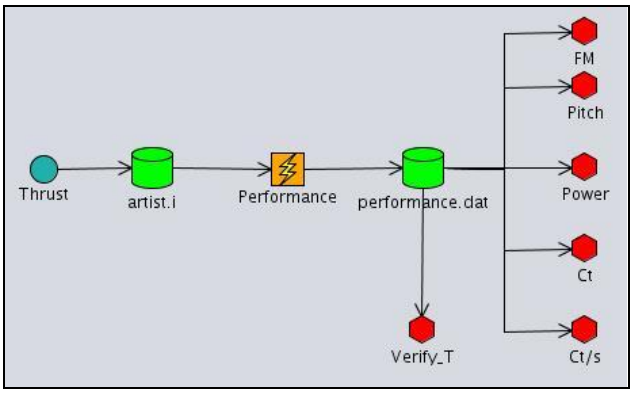

Figure 12: workflow for performance prediction in hover under sweeping thrust.

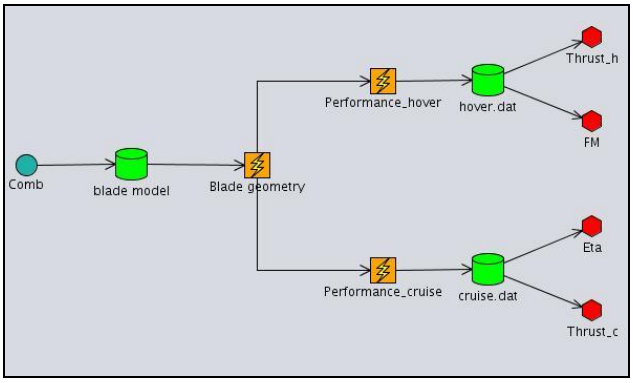

Figure 13: workflow for hover/cruise performance prediction.

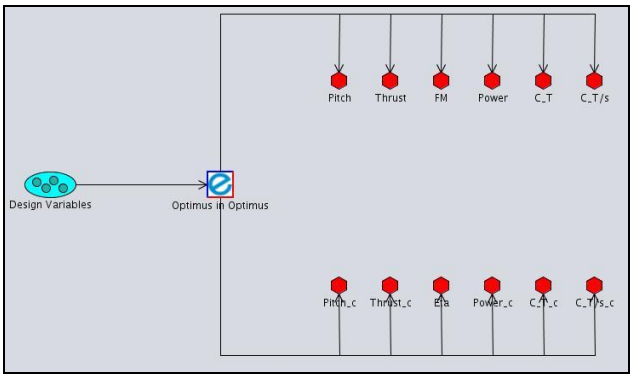

Figure 14: workflow for Optimus in Optimus® process.

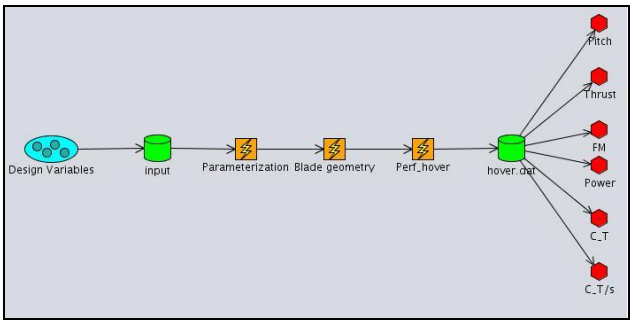

Figure 15: tasklist for hover performance in Optimus in Optimus®.

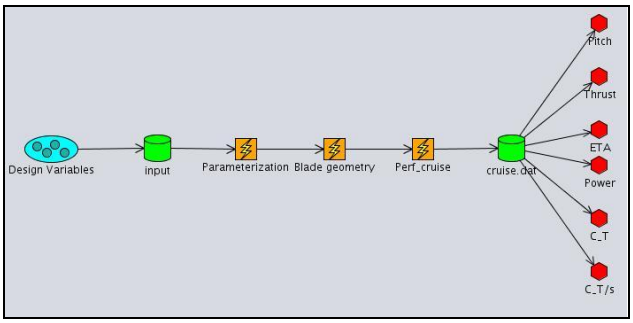

Figure 16: tasklist for cruise performance in Optimus in Optimus®.

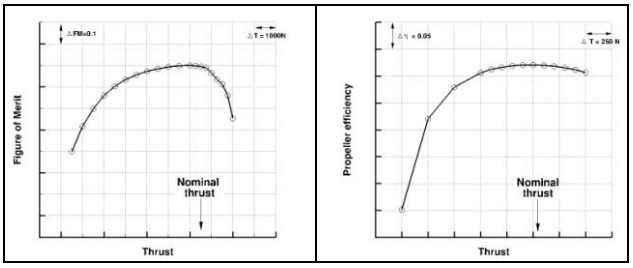

Figure 17: baseline rotor performance in hover (left) and cruise (right).

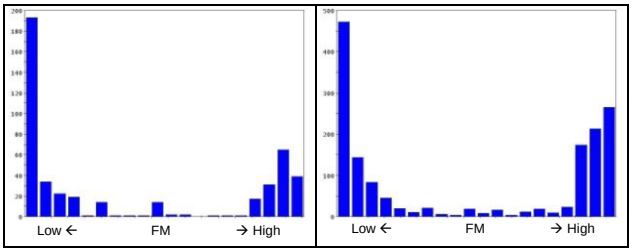

Figure 18: number of designs exceeding the nominal thrust in hover by 20% without morphing (left) and with morphing (right) for given values of Figure of Merit.

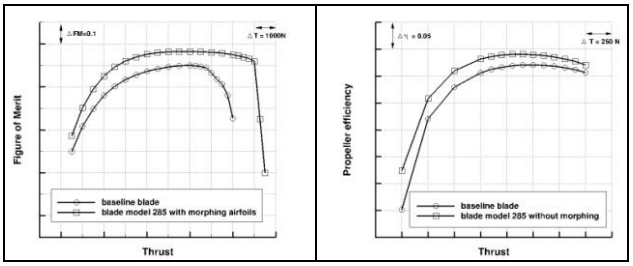

Figure 19: rotor performance of design 285 in hover (left) and cruise (right).

In order to find the optimal blade featured by a hover thrust 20% higher than the nominal value, a multi-objective optimization was performed by involving 10 design variables which act on blade planform parameters, twist, blade segments length, aerofoil distribution and morphed shapes.

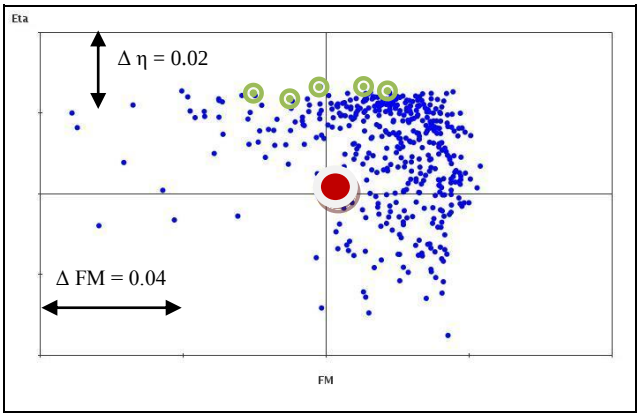

Figure 20: designs into the objectives plane. Green marks are for designs selected in Table 4. The red mark refers to the baseline blade at thrust nominal conditions.

Low and high bounds were set for geometrical entities (sectional chord, twist, sweep angle, …).

An evolutionary algorithm (NSEA+)[17] has been applied on an initial population of 1649 individuals (already computed) and the evaluation of thousands of additional designs was needed.

Figure 20 illustrates the designs into the objectives space showing that many designs reached the target. In that case, the main interest was not in the design performance but in the existence of blade models with their own aerofoil distributions (including morphed shapes) fulfilling the thrust requirements. The performance of the baseline blade at nominal thrust conditions has been added in Figure 20 and it serves only as reference. Table 4 collects the top five designs with the highest propeller efficiency. Table 4 also includes the aerofoil distribution from which it can be seen that the combination of LED and SETE generally results in better performance. It is important to emphasize that the blade is un-morphed when the rotor is in cruise flight and that it is supposed to morph only in hover.

The chord and twist distributions of design 681 are compared with the geometric characteristics of the baseline blade in Figure 21 and a 3D view, together with the aerofoil selection and distribution, is depicted in Figure 22.

Design	Aerofoil position from root to tip					
	1st	2nd	3rd	4th	5th	6th
681	A1	A2	A2	A3_07	A3_07	A5
683	A1	A2	A2	A3_09	A3_09	A5
1557	A1	A2	A2	A3_12	A3_12	A4
582	A1	A2	A3_12	A3_12	A4	A5
891	A1	A3_09	A3_09	A4	A5	A5

Table 4: aerofoil distribution for some noticeable designs.

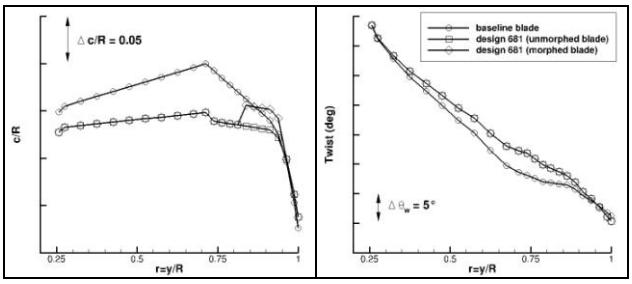

Figure 21: chord (left) and twist (right) distribution of design 681.

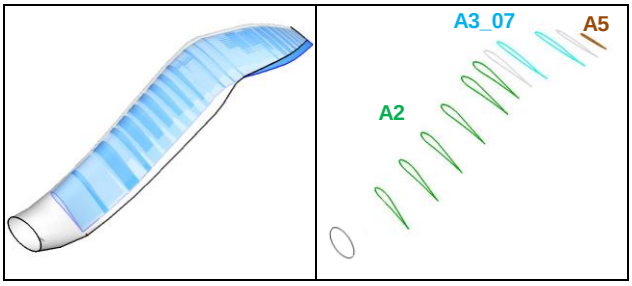

Figure 22: 3D view of design 681. On the left, the comparison with the baseline (grey shaded). On the right, the aerofoil distribution.

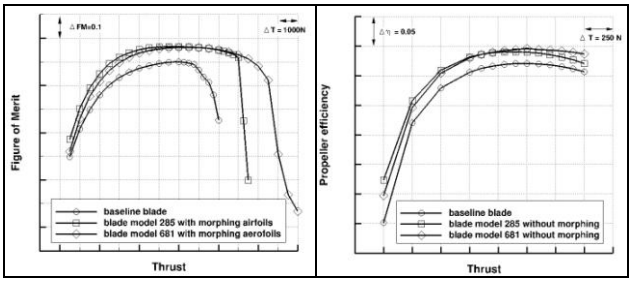

Figure 23: rotor performance of design 681 in terms of aerodynamic efficiency in hover (left) and cruise (right).

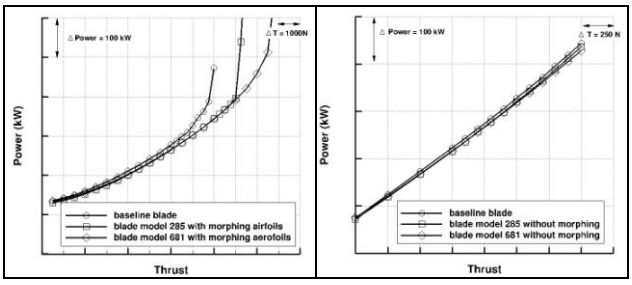

Figure 24: rotor performance of design 681 in terms of power in hover (left) and cruise (right).

The performance of design 681 is opposed to that one of the baseline blade and design 285 both in terms of aerodynamic efficiency (Figure 23) and in terms of power (Figure 24).

8. CONCLUSIONS

A methodology for the aerodynamic shape optimization of tiltrotor blades which exploits continuous morphing cross sections has been illustrated. It is based on several procedures executing a BEMT code embedded within a commercial optimization environment. Several tools have been developed to morph the sections and to distribute selected aerofoils on the blade planform. The fact that a blade was able to accommodate sections of different states (the un-morphed one plus several morphed ones) has led to the management of the design variables associated with those states.

The novelty of the present approach with respect to the state of the art consists in a unique optimization process which meets the aerodynamic performance objectives by selecting the most suitable aerofoil geometries, positioning them along the blade span, choosing the convenient morphing technology and determining the amount of the needed deformation. These features are in addition to the common practice of an optimization task based on planform related parameters and twist distribution.

The potential of the methodology has been discussed after performing both design space explorations and optimization tasks. The applications have been performed on a realistic case even though the nature of the present study was essentially exploratory. In fact, the applications did not emanate from an industrial project but they were intended to assess the methodology in light of forthcoming research projects.

The rotor of a convertiplane is a complex system that need to perform under varying operating conditions. The adoption of morphing devices may allow the rotor to produce a higher thrust in hover and the un-morphed blade is more aerodynamically efficient in cruise. The selection of the aerofoils to be mounted on a blade and especially their spanwise distribution (taking simultaneously into account that one of them is morphed in hover) have been object of solely aerodynamic considerations. Of course, the predicted benefits must be balanced with the complexity of the mechanisms and complemented by structural and power analyses. The existence in the design space of solutions based exclusively on aerofoil selection and spanwise placement, even if characterized by lower but still acceptable performance, may make the adoption of morphing sections less attractive.

The topics here discussed are stimulating the European research community since tiltrotor is one of the two rotorcraft concepts under development in the framework of the innovative aircraft demonstrator

platform (IADP) Fast Rotorcraft of the European Commission HORIZON 2020 Programme through the Joint Technology Initiative Clean Sky 2.

ACKNOWLEGMENTS

The baseline blade geometry and the corresponding aerodynamic experimental data were taken from the documentation of the ADYN project (2002-2007) partially funded by the European Commission under the 5th Framework Programme.

REFERENCES

[1] Thornburgh R P, Kreshock A R, Wilbur M L, Sekula M K, Shen J. Continuous Trailing-Edge Flaps for Primary Flight Control of a Helicopter Main Rotor. *Proceedings of the 70th* AHS *Annual Forum,* Montréal, Canada, 2014.

[2] Yokozeki T, Sugiura A and Hirano Y. Development of Variable Camber Morphing Airfoil Using Corrugated Structure. *Journal of Aircraft,* Vol. 51, No. 3, 2014.

[3] Khoshlahjeh M and Gandhi F. Extendable Chord Rotors for Helicopter Envelope Expansion and Performance Improvement, *Journal of the American Helicopter Society,* Vol. 59, No. 1, 2014.

[4] Murugan M S, Woods B K S and. Friswell M I. Morphing Helicopter Rotor Blades with Curvilinear Fiber Composites. *Proceedings of the 38th European Rotorcraft Forum*, Amsterdam, Netherlands, 2012.

[5] Barbarino S, Dettmer W G and Friswell M I. Morphing Trailing Edges with Shape Memory Alloy Rods. *Proceedings of the 21st International Conference on Adaptive Structures and Technologies (ICAST)*, University Park, Pennsylvania, 2010.

[6] Ameduri S. A Leading Edge Morphing Architecture for Droop Nose Effect. *Proceedings of the Italian Association of Aeronautics and Astronautics XXII Conference*, Naples, Italy, 2013.

[7] Jain R, Yeo H and Chopra I. Investigation of Trailing-Edge Flap Gap Effects on Rotor Performance Using High-Fidelity Analysis. *Journal of Aircraft,* Vol. 50, No. 1, 2013.

[8] Nannoni F, Giancamilli G and Cicalé M. ERICA: the European Advanced Tiltrotor. Proceedings of 27th European Rotorcraft Forum, Moscow, Russia, 2001.

[9] Porres E, De Vries H, Bauer M, Da-Rold M, De Nicola F, Zoppitelli E. DART Tilt Rotor Program Manufacturing And Tests Status. *Proceedings of 32nd European Rotorcraft Forum*, Maastricht, The Netherlands, 2006.

[10] Lefebvre T, Beaumier P, Canard S, Pisoni A, Pagano A, Sorrentino A, van der Wall B, D'Alascio A, Arzoumanian C, Voutsinas S and Hermans C. Aerodynamic and Aeroacoustic Optimization of Modern Tilt-Rotor Blades within the ADYN Project. *Proceedings of the ECCOMAS-2004 conference.* Jyvaskyla, Finland, 2004.

[11] www.nicetrip.onera.fr

[12] Decours J, Beaumier P, Khier W, Kneisch T, Valentini M and Vigevano L. Experimental Validation of Tilt-Rotor Aerodynamic Prediction. *Proceedings of 40th European Rotorcraft Forum*, Southampton, UK, 2014.

[13] Pagano A. Advanced Tiltrotor Blade Shapes by Multi-objective Optimization. *Proceedings of Eurogen 2011 Conference,* Capua (CE), Italy, 2011.

[14] Pagano A. Aerofoil Selection and Spanwise Placement in Aerodynamic Design and Optimization of Tiltrotor Blades. *Proceedings of the 39th European Rotorcraft Forum*, Moscow, Russia, 2013.

[15] Léon O, Hayden E, Gandhi F. Rotorcraft Operating Envelope Expansion Using Extendable Chord Sections. *Proceedings of the American Helicopter Society 65th Annual Forum*, Grapevine, Texas, May 27-29, 2009

[16] Khoshlahjeh M, Bae E S and Gandhi F. Helicopter Performance Improvement with Variable Chord Morphing Rotors, *Proceedings of 36th European Rotorcraft Forum*, Paris, France, 2010.

[17] Noesis Solutions (www.noesissolutions.com), Optimus rev. 10.15, 2014.

[18] Leishman J G and Nguyen K Q. State-Space Representation of Unsteady Airfoil Behaviour. *AIAA Journal*, Vol. 28, No. 5, pp. 836-844,1990.

[19] Stahlhut C and Leishman J G. Aerodynamic Design Optimization of Proprotors for Convertible-Rotor Concepts. *Proceedings of the 68th AHS annual forum*. Fort Worth, TX, 2012.

[20] Winarto H. BEMT Algorithm for the Prediction of the Performance of Arbitrary Propellers. *CR CoE-AL 2004-HW3-01*, Centre of Expertise in Aerodynamic Loads, Royal Melbourne Institute of Technology. Australia, 2004.

[21] www.esposa-project.eu

[22] Bianchi E, Preatoni G and Dalla Rovere N. Mach scaled wind tunnel tests on a 4-bladed half-span advanced Tilt-Rotor. *Proceeding of the American Helicopter Society 63rd Annual Forum*, Virginia Beach, VA, USA, 2007.

[23] Bianchi E and Beaumier P. Final Optimised Blade Design, Characteristics and Loads. ADYN consortium confidential report ADYN/WP3/AG/ D3-7/C, 2003.

[24] Eberhard A, and Salbashian C. NICETRIP rotor: an optimized tilt-rotor. *Proceedings of 69th AHS Annual Forum*, Phoenix, Arizona, 2013

[25] Decours J, Burguburu S and Falissard F. Performance Assessment of the Erica Tilt-Rotor in Cruise. *Proceeding of the 36th European Rotorcraft Forum*, Paris, France, 2010.

[26] Bae E S and Gandhi F. CFD Analysis of High-Lift Devices on the SC-1094R8 Airfoil. *Proceedings of 67th AHS Annual Forum*, Virginia Beach, VA, 2011.

[27] Jain R, Yeo H and Chopra I. Computational Fluid Dynamics–Computational Structural Dynamics Analysis of Active Control of Helicopter Rotor for Performance Improvement. *Journal of American Helicopter Society,* Vol. 45, 042004, 2010.

[28] Garcia-Duffy C, D'Andrea A and Melone S. Exploitation of Active Controls and Morphing Technologies to Enhance Rotor Aerodynamic Performance in Hover Conditions. *Proceedings of AHS Aeromechanics Specialist's Conference*, San Francisco, California, 2010.